Journal of Engineering Physics and Thermophysics, Vol. 82, No. 3, 2009

COMPARISON OF METHODS FOR WALL BOUNDARY CONDITIONS AS APPLIED TO THE CALCULATION OF TURBULENT HEAT EXCHANGE CHARACTERISTICS

K. N. Volkov

UDC 532.529

Methods for setting and realizing wall boundary conditions numerically in calculating turbulent flows is considered. A method for realizing weak boundary conditions on the wall with discretization of Reynolds-averaged Navier–Stokes equations by the control volume approach is discussed. The results of calculations for a number of model problems obtained within the framework of different approaches to the near-wall modeling are compared to the data of the physical experiment and the available correlation dependences. The grid dependence of the solution in using the method of near-wall functions is compared to that in using weak boundary conditions.

Keywords: *heat transfer, turbulence, boundary conditions, near-wall function method.*

Introduction. For a flexible description of regions of complex geometric configurations characteristic of engineering applications, numerical methods for calculating compressible turbulent flows on nonstructured grids are developed. Unlike the well-developed technologies of the finite element method, finite-volume technologies on nonstructured grids are characterized by the absence of single principles permitting discretization of convective and diffusion flows and source terms [1, 2].

Among the differential turbulence models used for closing Reynolds-averaged Navier–Stokes equations, the Spalart–Allmaras model [3] and the k–ε model [4] have found wide application. For modeling a flow in the near-wall region several approaches are used: the near-wall function method ($y^+ \sim 10$), low-Reynolds turbulence models ($y^+ < 1$), and a two-layer model ($y^+ \sim 1$).

In the near-wall function method, the viscous sublayer and the transition zone of the boundary layer are not resolved but are described by semiempirical formulas (near-wall functions). The accuracy is increased by solving simplified equations of the boundary layer in the near-wall control volume [5]. An increase in the grid resolution near the wall usually leads to a higher accuracy.

Attempts to widen the range of application of the k–ε model [4] up to the wall, including the viscous sublayer (on the condition of the necessary resolution of the grid in the boundary layer) led to the creation of its low-Reynolds versions differing in the form of recording source terms, wall boundary conditions, and damping functions [6].

The Spalart-Allmaras model [3] is a low-Reynolds model that requires a proper resolution of the near-wall zone of the boundary layer. At the same time the Spalart-Allmaras model is also used in combination with the near-wall function method in the case of a rather rough grid.

The two-layer model is a compromise variant between the high- and low-Reynolds turbulence models [7]. The near-wall region is subdivided into two subregions — interior and exterior — the boundary between which depends on the local Reynolds number. In the exterior, equations of the model of [4] and in the interior the model of [8] are used.

For the normal wall velocity, as a rule, the boundary nonpercolation condition $\mathbf{v}_n = 0$ is used, and for the tangential velocity one uses the adhesion condition $\mathbf{v}_\tau = 0$ (severe boundary conditions). Despite the fact that the setting of the sliding condition on the wall $\mathbf{v}_\tau \neq 0$ (weak boundary conditions) contradicts the physical reality (rarefied flows are not considered) such an approach is used in computational practice but mainly in discretizing Navier–Stokes equations by the finite element method [9]. The influence of the wall on the flow is taken into account in the form of grid shear stresses and additional grid generation of turbulence due to the difference of the tangential velocity profile from the logarithmic distribution near the wall [1, 2].

University of Surrey, Guildford, GU27XH, Great Britain; email: dsci@mail.ru. Translated from Inzhenerno-Fizicheskii Zhurnal, Vol. 82, No. 3, pp. 471–480, May–June, 2009. Original article submitted July 17, 2007.

The present paper considers methods for setting and realizing numerically weak boundary conditions on the wall in the calculations of turbulent flows on nonstructured grids. To close Reynolds-averaged Navier–Stokes equations, the Spalart-Allmaras model and the k–ε model in combination with the near-wall function method and weak boundary conditions, as well as a two-layer model are used. The possibilities of the developed approach are demonstrated with the example of solving a series of model problems of gas dynamics and heat transfer. The influence of the near-wall grid pitch on the accuracy of calculations is shown, and the grid dependence of the solution in using the near-wall function method and weak boundary conditions is investigated.

Basic Equations. In the Cartesian coordinate system (x, y, z), the nonstationary flow of a viscous compressible gas is described by the equation

$$\frac{\partial \mathbf{Q}}{\partial t} + \frac{\partial \mathbf{F}}{\partial x} + \frac{\partial \mathbf{G}}{\partial y} + \frac{\partial \mathbf{H}}{\partial z} = \mathbf{S}. \tag{1}$$

Equation (1) is supplemented by the equation of state of an ideal gas

$$p = (\gamma - 1)\,\rho\left[e - \frac{1}{2}\left(u^2 + v^2 + w^2 - \omega^2 r^2\right)\right].$$

The vector of conservative variables and the flow vectors have the following form:

$$\mathbf{Q} = \begin{pmatrix} \rho \\ \rho u \\ \rho v \\ \rho w \\ \rho e \end{pmatrix}, \quad \mathbf{F} = \begin{pmatrix} \rho u \\ \rho uu + p - \tau_{xx} \\ \rho uv - \tau_{xy} \\ \rho uw - \tau_{xz} \\ (\rho e + p)\,u - u\tau_{xx} - v\tau_{xy} - w\tau_{xz} + q_x \end{pmatrix},$$

$$\mathbf{G} = \begin{pmatrix} \rho v \\ \rho vu - \tau_{yx} \\ \rho vv + p - \tau_{yy} \\ \rho vw - \tau_{yz} \\ (\rho e + p)\,v - u\tau_{yx} - v\tau_{yy} - w\tau_{yz} + q_y \end{pmatrix}, \quad \mathbf{H} = \begin{pmatrix} \rho w \\ \rho wu - \tau_{zx} \\ \rho wv - \tau_{zy} \\ \rho ww + p - \tau_{zz} \\ (\rho e + p)\,w - u\tau_{zx} - v\tau_{zy} - w\tau_{zz} + q_z \end{pmatrix}.$$

The noninertiality of the reference system is taken into account by introducing into the source term the Coriolis and centrifugal force

$$\mathbf{S} = \begin{pmatrix} 0 \\ 0 \\ \rho\omega\,(y\omega + 2w) \\ \rho\omega\,(z\omega - 2v) \\ 0 \end{pmatrix}.$$

The tensor components of viscous stresses and the vector components of the heat flow are found from the relations

$$\tau_{xy} = \mu_e\left(\frac{\partial v_x}{\partial x_y} + \frac{\partial v_y}{\partial x_x} - \frac{2}{3}\frac{\partial v_k}{\partial x_k}\right), \quad q_x = -\lambda_e\frac{\partial T}{\partial x_x}.$$

Equation (1) is suitable for describing both laminar and turbulent flows. In modeling turbulent flows, Eq. (1) is supplemented by turbulence model equations. In so doing, the effective viscosity is calculated as a sum of molecular and turbulent viscosities, and the effective heat conductivity is expressed in terms of the viscosity and the Prandtl number. To obtain molecular viscosity values depending on the temperature, the Sutherland law is used. The molecular and turbulent Prandtl numbers are given constant values (for air Pr = 0.72, $\mathrm{Pr_t}$ = 0.9).

Turbulence Model Equations. To close Reynolds-averaged Navier–Stokes equations, we use the Spalart-Allmaras model and the k–ε model in combination with the near-wall function method or weak boundary conditions, as well as a two-layer model.

Spalart-Allmaras model. The Spalart-Allmaras model involves the solution of the differential equation for the working variable connected with the turbulent viscosity [1]. The source term is calculated on the basis of the vorticity.

Dissipative model. In the k–ε model, differential equations for the kinetic energy of turbulence and its dissipation rate are solved [4]. The turbulence production term is found with account for the Kato–Launder modification. The turbulent viscosity is calculated by the Kolmogorov–Prandtl formula.

Near-wall function method. Near-wall functions represent a set of semiempirical formulas relating the sought functions in the near-wall control volume to the corresponding quantities on the wall.

In the turbulent boundary layer, one usually distinguishes several characteristic subregions using the distance from the wall $y^+ = \rho y u_*/\mu$ and the velocity $u^+ = u/u_*$ given in near-wall units where $u_* = \tau_w/\rho^{1/2}$. In the viscous sublayer, viscous stresses dominate over Reynolds stresses, and a linear dependence of the velocity on the distance to the wall $u^+ = y^+$ (at $0 < y^+ < 11$) takes place. In the logarithmic layer, Reynolds stresses considerably exceed viscous stresses, and the velocity profile is described by the logarithmic law $u^+ = (1/\kappa)\ \ln\ (Ey^+)$ (at $11 < y^+ < 28$). For a smooth wall $E = 8.8$.

The distribution of shear stresses is assumed homogeneous within the near-wall control volume. Shear stresses on the wall are calculated by the formula $\tau_w = \mu_e \Delta u A/\Delta y$, where Δu and Δy are the differences of tangential velocities and coordinates between the wall and the near-wall node. Taking into account that $\mu_e = \mu \mathrm{Re}/u^{+2}$, where $\mathrm{Re} = \rho \Delta u \Delta y/\mu = u^+ y^+$, we obtain $\tau_w = \rho \Delta u^2/u^{+2}$.

The velocity u^+ is obtained by means of the iteration procedure on the basis of the Newton method [1, 2].

Weak boundary conditions. Weak boundary conditions are realized through the calculation of the tangential velocity on the wall, which is added to the residual caused by the discretization of nonviscous flows through the faces of the near-wall control volume [1, 2].

Tangential velocities on the wall are found form the relations

$$u_{\tau 1} = u_{\tau 2} - \tau_x \frac{\Delta u}{\mu_e}, \quad v_{\tau 1} = v_{\tau 2} - \tau_y \frac{\Delta u}{\mu_e}, \quad w_{\tau 1} = w_{\tau 2} - \tau_z \frac{\Delta u}{\mu_e},$$

where

$$\tau_x = \tau_w \frac{u_{\tau 2} - u_{\tau 1}}{\Delta u}; \quad \tau_y = \tau_w \frac{v_{\tau 2} - v_{\tau 1}}{\Delta u}; \quad \tau_z = \tau_w \frac{w_{\tau 2} - w_{\tau 1}}{\Delta u}.$$

The tangential velocity components $\{u_\tau, v_\tau, w_\tau\}$ in the local coordinate system are related to the Cartesian velocity components $\{u, v, w\}$ by the relations $u_\tau = u - v_n n_x$, $v_\tau = v - v_n n_y$, $w_\tau = w - v_n n_z$, where $v_n = u n_x + v n_y + w n_z$ is the velocity on the normal to the face of the control volume.

The logarithmic velocity profile extends to the wall (the viscous sublayer is not resolved, as in the case of the near-wall function method). The tangential velocity on the wall is obtained by averaging over the logarithmic velocity distribution in the near-wall control volume (Fig. 1). The shaded part corresponds to the domain used for averaging over the logarithmic velocity profile.

Modified values of the tangential velocity on the wall are found from the relations

$$u^*_{\tau 1} = u_b \frac{u_{\tau 2} - u_{\tau 1}}{\Delta u}, \quad v^*_{\tau 1} = u_b \frac{v_{\tau 2} - v_{\tau 1}}{\Delta u}, \quad w^*_{\tau 1} = u_b \frac{w_{\tau 2} - w_{\tau 1}}{\Delta u}. \tag{2}$$

The values of (2) are used to calculate the residual caused by the discretization of nonviscous flows. The flow velocity in the boundary layer $u_b = \mu u_b^+ \rho \Delta y$ given in near-wall units is calculated with the use of the wall law [2] whose integration yields

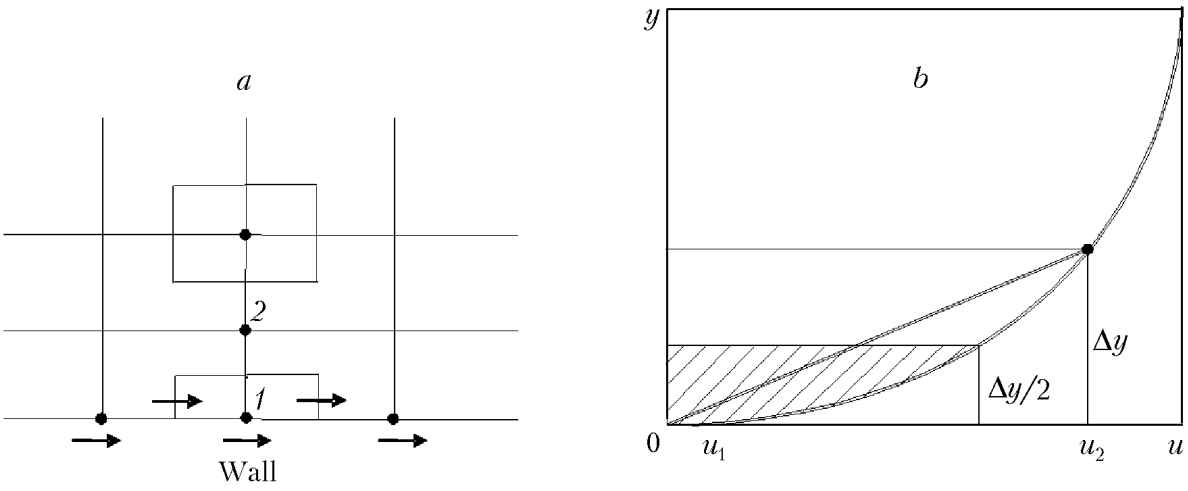

Fig. 1. Near-wall control volume (a) and velocity profile in the boundary layer (b): 1) near-wall control volume; 2) next volume.

$$u_{\mathrm{b}}^{+} = u^{+}y^{+} - \frac{1}{2}u^{+2} + \frac{1}{\kappa}(u^{+} - y^{+}) + \frac{1}{24\kappa E}(\kappa u^{+})^{4},$$

where $y^{+} = \mathrm{Re}/u^{+}$. The nonlinear equation defining u^{+} is solved with the help of the Newton method [1, 2].

From the point of view of the program realization, the calculation of the tangential velocity is included in the procedure of discretization of nonviscous flows and requires comparatively small modifications of the code [10] based on the near-wall function method.

Two-layer model. The near-wall region is subdivided into two subregions — interior and exterior, the boundary between which depends on the local Reynolds number $\mathrm{Re}_y = \rho k^{1/2} y/\mu$. At $\mathrm{Re}_y > \mathrm{Re}_y^{*}$ the k–ε model is used and the turbulent viscosity is calculated by the Kolmogorov–Prandtl formula [7]. At $\mathrm{Re}_y < \mathrm{Re}_y^{*}$ the model of [8] is used. It is assumed that $\mathrm{Re}_y^{*} = 180$. To provide a smooth transition, the transition function $\chi = (220 - \mathrm{Re}_y)/40$ (at $180 < \mathrm{Re}_y < 220$) is introduced.

As a wall boundary layer for the kinetic turbulence energy, the Neumann condition ($\partial k/\partial y = 0$) is taken. The boundary condition for the dissipative function on the wall is not needed.

Numerical Method. Discretization of Eq. (1) and turbulence model equations is carried out with the use of the finite volume method [10] in which a control volume centered with respect to a grid node is used.

For time discretization, the 5th-order Runge–Kutta method is used. For discretization of nonviscous flows, the MUSCL scheme (Monotone Upstream-centered Scheme for Conservation Laws) and for discretization of viscous flows, the 2nd-order finite difference formulas are used. The system of difference equations is solved by a multigrid method on the basis of the full approximation scheme. The sequence of embedded grids is constructed with the use of the method of collapsing faces [10].

Results of the Calculations. Comparison of different methods for near-wall modeling is made on the basis of the solution of a series of model problems among which are the flow in the boundary layer on a flat plate with a zero and a negative pressure gradient, as well as the heat transfer of a freely rotating disc.

At the initial instant of time the gas is at rest. As a working medium, air (whose thermophysical properties are reference properties) is taken.

Boundary layer with a zero pressure gradient. For the flow in the boundary layer on a flat plate with a zero pressure gradient, reliable experimental and calculated data are available [11, 12] (the results were obtained for an incompressible fluid at $\mathrm{M}_{\infty} < 0.2$).

The length of the calculation region is 100 mm and its width is 20 mm. Calculations are performed on a 35×32 grid with a crowding of nodes towards the front edge and the surface of the plate (Fig. 2). In so doing, $y^{+} \sim 8$, which is comparable to the grid used [12].

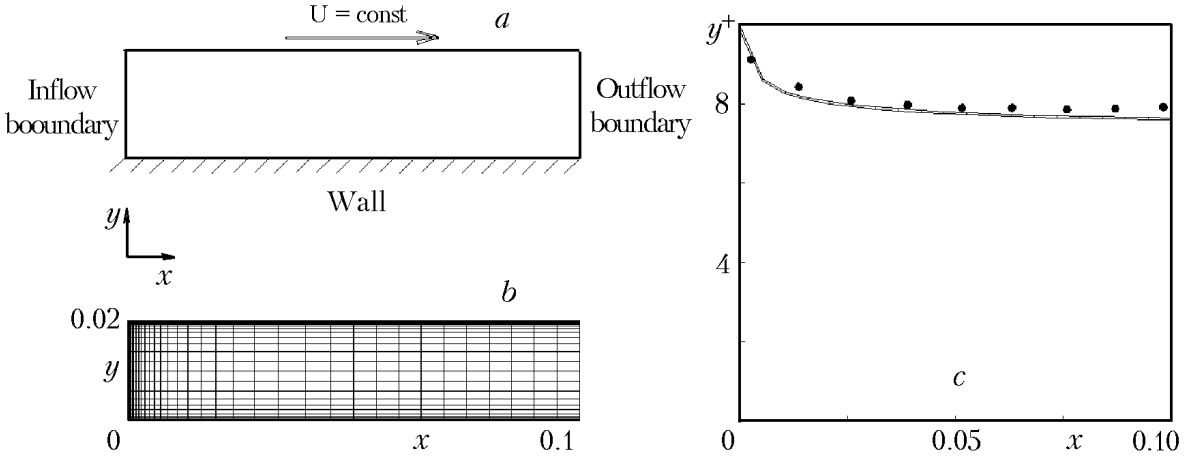

Fig. 2. Geometry of the computational domain (a), grid (b), and coordinate y^+ distribution along the plate surface (c). Dots correspond to the grid used in [12]. x, y, m.

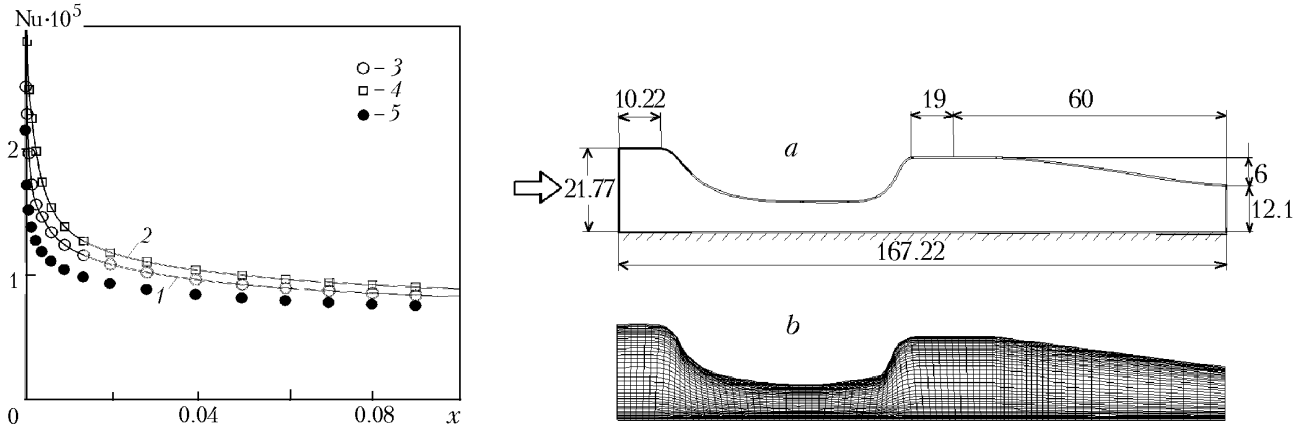

Fig. 3. Distribution of the Nusselt number along the plate surface: 1) and 2) results of calculations by the k–ε model and the Spalart–Allmaras model in using serve boundary conditions; 3) and 4) results of calculations by the k–ε model and the Spalart–Allmaras model in using weak boundary conditions; 5) data of [11].

Fig. 4. Geometry of the computational domain in (a) and grid with 40 nodes in the transverse direction (b).

In the inlet cross-section, the total pressure, the total temperature, and the turbulence characteristics are given ($p_{0\infty} = 6.67 \cdot 10^5$ Pa, $T_{0\infty} = 400$ K, $k_\infty = 2$ m^2/sec^2, $\varepsilon_\infty = 200$ m^2/sec^3, which corresponds approximately to $U_\infty = 200$ m/sec and $M_\infty = 0.5$). In the outlet cross-section, static pressure is taken ($p = 5.56 \cdot 10^5$ Pa). The wall temperature is assumed to be fixed ($T_w = 222.22$ K). At the upper boundary, boundary sliding conditions are set.

The distributions of the Nusselt number $\mathrm{Nu} = q_w x/(\lambda \Delta T)$, where $\Delta T = \Delta T_\infty - T_w$) given in Fig. 3 show that calculations give somewhat higher values of the heat transfer coefficient near the front edge of the plate as compared to the measurement data. On the whole, however, the agreement between the calculated and experimental data [11] is fairly good and demonstrates a weak dependence on the turbulence model and the approach to the simulation of the flow in the near-wall region.

Boundary layer with a negative pressure gradient. Experimental and calculated data for the flow in the boundary layer with a favorable and an unfavorable pressure gradient were obtained in [13, 14].

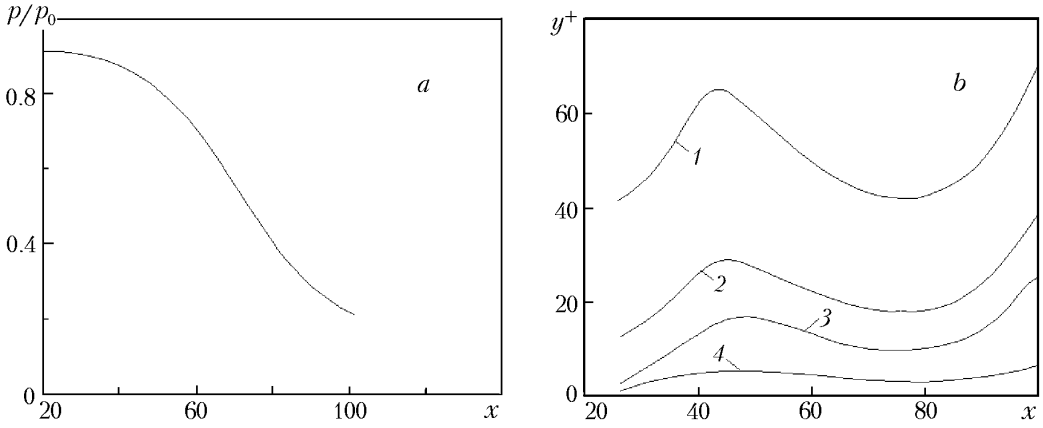

Fig. 5. Distribution of the pressure (a) and the near-wall coordinate y^+ (b) along the plate for grids with 40 (1), 60 (2), 80 (3), and 120 (4) nodes in the transverse direction. x, mm.

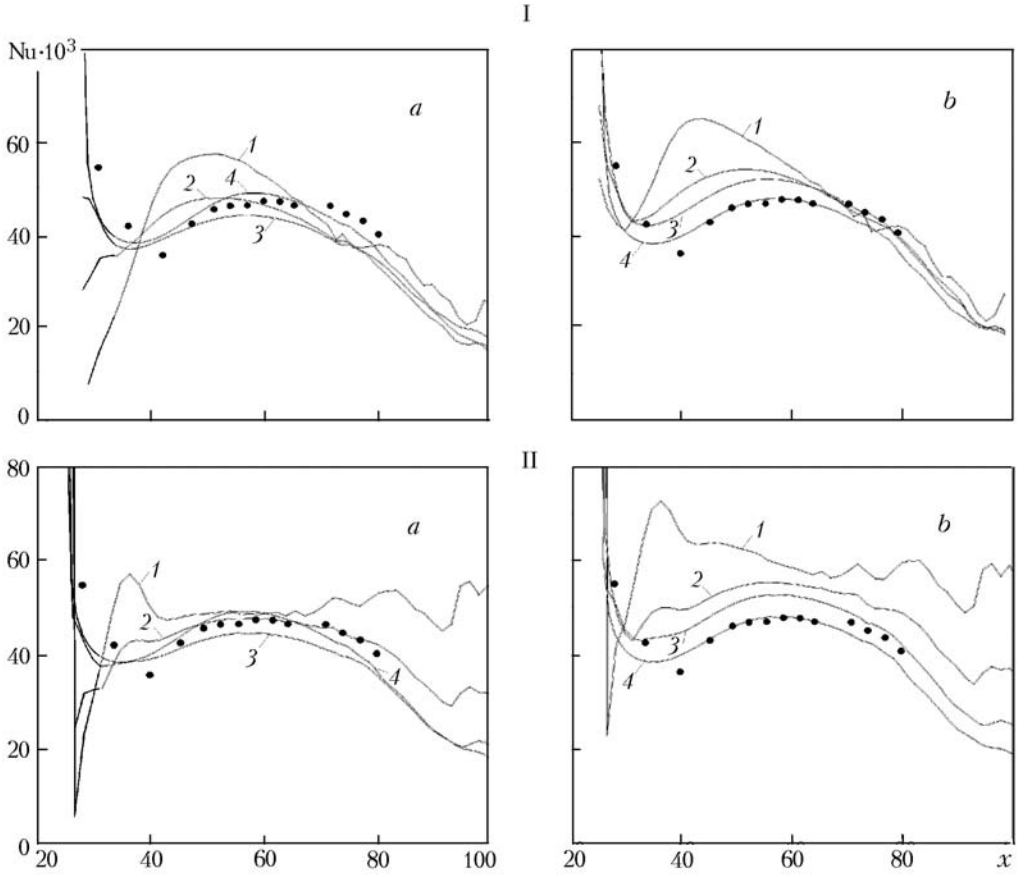

Fig. 6. Distributions of the local Nusselt number along the plate for the k–ε model (a) and the Spalart–Allmaras model (b) in using the near-wall function method (I) and at weak boundary conditions (II). x, mm.

The computational domain represents a curvilinear channel (Fig. 4, dimensions are given in millimeters). The lower wall is the surface of the plate, and the upper wall consists of segments of straight lines and circular arcs and is constructed so as to represent the pressure gradient created by the experimental facility [13] (Fig. 5a). Except for the small initial portion, a practically linear pressure distribution along the x coordinate is observed. The last section

(at $x > 120$ mm) is made narrowing to guarantee convergence of the numerical solution. At the given parameters the flow in the outlet cross-section is supersonic and, therefore, the features of the downstream flow from the above cross-section have no influence on the parameters of the upstream flow.

In the inlet cross-section, we give the total pressure ($p_{0\infty} = 3.66 \cdot 10^5$ Pa), the drag temperature ($T_{0\infty} = 380$ K), the kinetic energy of turbulence and the rate of its dissipation ($k_\infty = 2$ m^2/sec^2, $\varepsilon_\infty = 200$ m^2/sec^3), and in the outlet cross-section — the static pressure ($p = 1.013 \cdot 10^5$ Pa). The upper wall is assumed to be heat-insulated ($\partial T/\partial n = 0$). The plate has a constant temperature ($T_w = 365$ K).

In the calculations, several grids characterized by different values of the y^+ coordinate are used (Fig. 5b). At 40, 60, and 80 nodes across the channel the grid contains 2800, 4200, and 7200 nodes, respectively. The grid containing 20,000 nodes is used for calculations on the basis of the two-layer model (the grid has 120 nodes in the transverse direction).

The local Nusselt number is found from the relation $\mathrm{Nu} = q_w/(\lambda \Delta T)$, where $\Delta T = T_{0\infty} - T_w$ (the characteristic linear size is taken to be equal to 1). The thermophysical parameters are calculated at $T = T_{0\infty}$.

The Nusselt number distributions are shown in Fig. 6 for the near-wall function method and weak boundary conditions. Curves 1–3 correspond to calculations on grids with 40, 60, and 80 nodes in the transverse direction, curve 4 corresponds to the calculation by the two-layer model, and dots — to the data of the physical experiment [13].

With receding from the front edge of the plate the Nusselt number first decreases (its minimum takes place at $x \sim 38$ mm) and then reaches its maximum again. Distributions described by curves 1 in Fig. 6 I give a significant error in the position of the local maximum of the Nusselt number, which is explained by the low values of y^+ near the wall. The accuracy of the results obtained on the basis of the Spalart–Allmaras model and the k–ε model with near-wall functions is recognized as unsatisfactory. At the same time the two-layer model gives results that are in good agreement with the data of the physical experiment [13] and the calculated data [14] but require a 20% increase in the number of grid nodes and in the counting time. The weak boundary conditions show a good convergence rate of the interaction process and good results for the accuracy, except for the coarsest grid (curves 1 in Fig. 6 II).

Heat transfer of the rotating disc. Consider the heat transfer on a flat disc uniformly rotating with angular velocity ω about the axis perpendicular to its plane.

The geometrical model represents a sector with an opening angle of 3° (Fig. 7). The inner radius of the disc $r_i = 76$ mm, the outer radius $r_o = 475$ mm, and its width $l = 35$ mm. The length of the computational domain is chosen to be equal to $r_d = 2r_o$.

The disc has a constant temperature $T_w = 420$ K and rotates with an angular velocity $\omega = 200$ 1/sec, which corresponds to $\mathrm{Re} = 3.1 \cdot 10^6$. On the bush surface the sliding conditions are given. On the far boundary $p_\infty = 1.013 \cdot 10^5$ Pa, $k_\infty = 1$ m^2/sec^2, $\varepsilon_\infty = 10$ m^2/sec^3. In the peripheral direction periodic boundary conditions are set.

Calculations are performed on coarse and detailed grids containing 22,062 and 43,062 nodes, respectively (on the disc surface 40 and 60 nodes are situated). For the coarse grid $y^+ = 8$–75 (three nodes are situated at $y^+ < 18$), and for the detailed grid $y^+ = 3$–29 (and $y^+ \sim 10$ is situated thereby on 1/3 of the disc surface). Both grids in the peripheral direction have one layer of cells. The coarse grid is shown in Fig. 8.

The Nusselt number is calculated by the formula $\mathrm{Nu}_r = q_w r/(\lambda \Delta T)$. At high Reynolds numbers when the heating of the disc due to friction becomes considerable, in determining the temperature difference ΔT, instead of the wall temperature T_w the adiabatic temperature of the disc $T_a = T_\infty + R\omega^2 r^2/(2c_p)$ is used. The recovery factor is taken to be equal to $R = \mathrm{Pr}^{1/3}$.

The results of the calculations by the k–ε model are presented in Fig. 9 in comparison with the experimental data of [15] (5) and the data of the theory of [16] (6) based on the Reynolds analogy between the momentum and heat transfer at a quadratic temperature distribution along the radius.

Calculations on the coarse grid give values of the Nusselt number 25–30% lower and on the detailed grid 16–25% lower compared to the measurement data. In using the near-wall function method and weak boundary conditions the discrepancy between the results on the maximum value of the Nusselt number is 2–8%. The theory of [16] predicts thereby a monotonic temperature distribution along the radius. The results of the calculations describe fairly well the theoretical dependence at $r/r_o < 0.9$. The nonmonotonic distribution of the Nusselt number is explained by the end effects and the formation of the recirculation flow zone at $r/r_o > 0.9$.

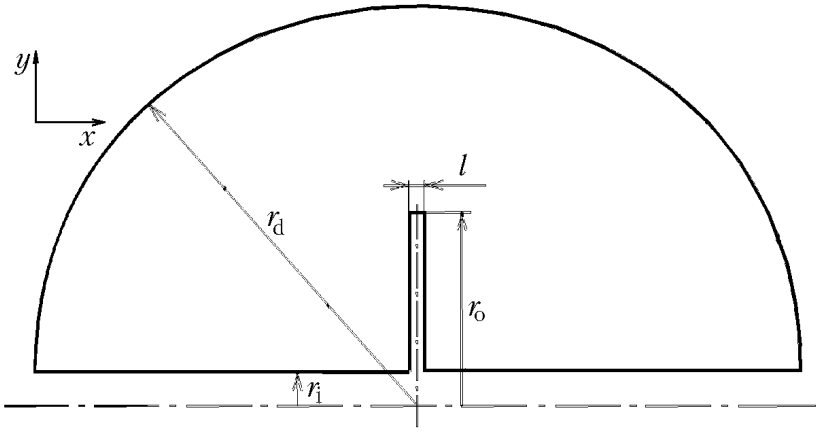

Fig. 7. Geometry of the computational domain.

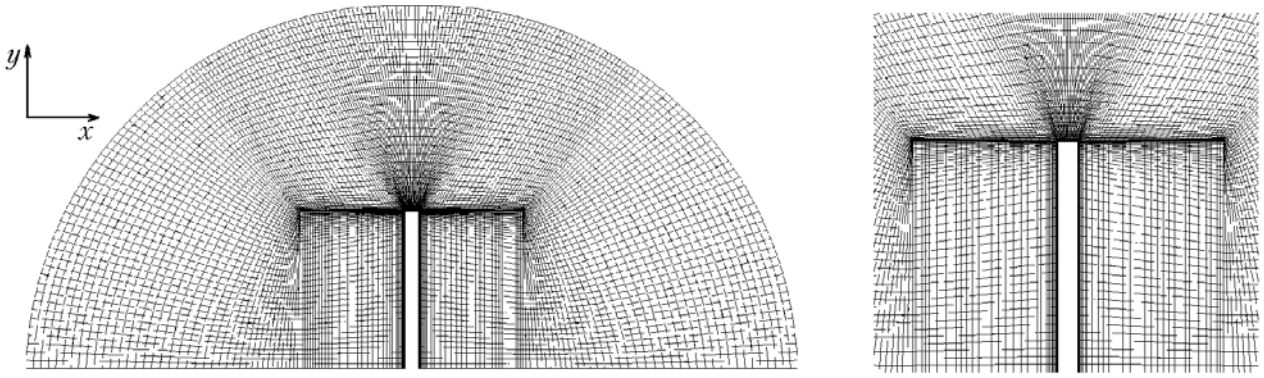

Fig. 8. Coarse grid near the disc.

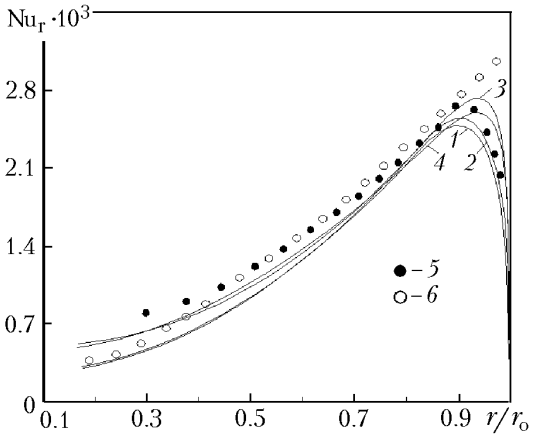

Fig. 9. Distributions of the local Nusselt number along the disc radius: 1 and 2) correspond to the coarse grid, and 3 and 4) to the detailed grid (1 and 3 were obtained on the basis of the near-wall function method, and 2 and 4 — at weak boundary conditions); 5) data of [15]; 6) data of [16].

Conclusions. The grid dependence of the solution in using the near-wall function method and weak boundary conditions has been investigated on a series of gas dynamics problems.

Weak boundary conditions have a number of advantages over the near-wall function method, among which are the comparatively simple approach to the program realization by using different turbulence models, the possibility

of using a coarser grid in the near-wall region, and the weakening of the grid dependence of the solution. In this case, there is also no need to realize the procedure of near-wall modeling for the temperature.

The chief disadvantage of weak boundary conditions is the fact that they are numerical and have no physical substantiation. It should be noted thereby that near-wall functions are also used in situations in which the wall law is inapplicable (e.g., for calculating boundary layers subjected to the influence of a pressure gradient or in the case where the values of the near-wall coordinate y^+ are lower than the recommended value).

The results of the calculations are important for investigating and controlling the heat exchange of the vanes of gas-turbine plants.

NOTATION

A, area, m^2; c_p, specific heat capacity at a constant pressure, J/(kg·K); e, total energy of a mass unit, J/kg; E, constant in the wall law; **F**, **G**, **H**, vectors of flows; k, kinetic energy of turbulence, m^2/sec^2; l, thickness of the disc, m; M, Mach number; **n**, n, normal vector and its absolute value; Nu, Nusselt number; p, pressure, Pa; Pr, Prandtl number; q, heat flow density, W/m^2; **Q**, vector of conservative variables; r, radius, m; R, recovery factor; Re, Reynolds number; **S**, source term; t, time, sec; T, temperature, K; u, v, w, velocity components, m/sec; U, velocity, m/sec; **v**, velocity vector, m/sec; x, y, z, Cartesian coordinates, m; γ, heat capacity ratio; δ, boundary layer thickness, m; δ_{ij}, Kronecker symbol; ε, dissipation rate of turbulence energy, m^2/sec^3; κ, Von Kármán constant; λ, heat conductivity, W/(m·K); μ, dynamic viscosity, kg/(m·sec); ρ, density, kg/m^3; τ, shear stress, N/m^2; χ, transition function; ω, angular velocity, 1/sec. Subscripts: a, adiabatic; b, boundary layer; d, computational domain; e, effective; i, inner; n, projection on the normal; o, outer; r, radial; t, turbulent; x, y, z, projections on the coordinate axes; w, wall; τ, projection on the tangent; 0, drag parameters; 1, near-wall node; 2, node closest to the wall; *, critical; +, dimensionless parameters in the boundary layer.

REFERENCES

1. K. N. Volkov, Boundary conditions on the wall in calculations of turbulent flows on nonstructured grids and the grid dependence of a solution, *Vychisl. Metody Programmir.*, **7**, 211–223 (2006).
2. K. N. Volkov, Near-wall modeling in calculations of turbulent flows on nonstructured grids, *Teplofiz. Aéromekh.*, **14**, No. 1, 113–129 (2007).
3. P. R. Spalart and S. R. Allmaras, A one-equation turbulence model for aerodynamic flows, *AIAA Paper*, No. 92-0439 (1992).
4. B. E. Launder and D. B. Spalding, The numerical computation of turbulent flows, *Comput. Meth. Appl. Mech. Eng.*, **3**, 269–289 (1974).
5. J. Bredberg, *On the Wall Boundary Condition for Turbulence Model*, Chalmers University of Technology, Internal Report 00/4, Sweden, Goteborg (2000).
6. K. N. Volkov, Comparison of low-Reynolds models of turbulence with the data of direct numerical simulation of the flow in a channel, *Teplofiz. Aéromekh.*, **12**, No. 3, 365–378 (2005).
7. W. Rodi, Experience with two-layer models combining the k–ε-model with one-equation model near wall, *AIAA Paper*, No. 91-0216 (1991).
8. M. Wolfshtein, The velocity and temperature distribution of one-dimensional flow with turbulence augmentation and pressure gradient, *Int. J. Heat Mass Transfer*, **12**, 301–318 (1969).
9. S. S. Collis, *Discontinuous Galerkin Methods for Turbulence Simulation*, Stanford University, Technical Report, USA, Stanford (2002).
10. K. N. Volkov, Application of the control volume method for solving problems of the mechanics of liquids and gases on nonstructured grids, *Vychisl. Metody Programmir.*, **6**, 43–60 (2005).
11. K. Wieghardt and W. Tillman, *On the Turbulent Friction Layer for Rising Pressure*, NACA Report, No. TM-1314 (1951).
12. D. A. Yoder and N. J. Georgiadis, Implementation and validation of the Chien k–ε-turbulence model in the WIND Navier–Stokes code, *AIAA Paper*, No. 99-0745 (1999).

13. A. J. H. Teekaram, C. J. P. Forth, and T. V. Jones, Film cooling in the presence of mainstream pressure gradients, *ASME J. Turbomachinery*, **113**, 484–492 (1991).
14. K. N. Volkov, Influence of pressure gradients and localized injection on the turbulent heat exchange of a flat plate, *Teplofiz. Vys. Temp.*, **44**, No. 3, 24–32 (2006).
15. A. Northrop and J. M. Owen, Heat transfer measurements in rotating-disc systems. Pt. 1: The free disc, *Int. Heat Fluid Flow*, **9**, No. 1, 19–26 (1988).
16. L. A. Dorfman, *Hydrodynamic Resistance and Heat Loss of Rotating Solids*, Edinburgh, Oliver & Boyd (1963).